Journal of Molecular Catalysis A: Chemical 338 (2011) 44–50

Contents lists available at ScienceDirect

Journal of Molecular Catalysis A: Chemical

journal homepage: www.elsevier.com/locate/molcata

A DFT study on the adsorption and dissociation of methanol over MoS_2 surface

Yan-Yan Chen[a,b], Mei Dong[a], Zhangfeng Qin[a], Xiao-Dong Wen[a], Weibin Fan[a], Jianguo Wang[a,*]

[a] State Key Laboratory of Coal Conversion, Institute of Coal Chemistry, Chinese Academy of Sciences, P.O. Box 165, Taiyuan, Shanxi 030001, PR China
[b] Graduate School of the Chinese Academy of Sciences, Beijing 100049, PR China

ARTICLE INFO

Article history:
Received 16 June 2010
Received in revised form 18 January 2011
Accepted 24 January 2011
Available online 1 February 2011

Keywords:
DFT
Methanol
Adsorption
Dissociation
MoS_2

ABSTRACT

The adsorption and subsequent dissociative reaction of methanol on the bald Mo-edge, 50% Mo-edge, and 50% S-edge of MoS_x clusters were investigated by using density functional theory (DFT). The calculation results showed that the adsorption of methanol molecule through its oxygen atom prefers the corner sites to the edge sites of MoS_x surfaces. The pathways of methanol dissociation via C–H, C–O and O–H bond scissions are considered and O–H bond scission is found to be the most favorable pathway on the MoS_2 surface; the activation barrier is 0.45 eV on the bald Mo-edge and about 1.0 eV on the 50% Mo-edge and 50% S-edge. Among the intermediates formed from methanol dissociation, CH_3O is the dominant surface species after the MoS_2 surface is exposed to methanol.

1. Introduction

Methanol is an excellent fuel on its own and can also be readily converted to hydrogen, formaldehyde, methyl formate, dimethyl ether, dimethoxymethane, olefins and alkenes via decomposition, dehydration and partial oxidation [1–4]. Moreover, it is also a precursor for the C–C bond formation during the higher alcohol synthesis and the Fischer–Tropsch synthesis on Cu/ZnO catalysts and MoS_2 catalysts [5–11]. Therefore, the dissociation and conversion of methanol has attracted great interests of researchers.

Methanol dissociation can proceed via three routes involving the breaking of O–H, C–O, and C–H bonds, respectively. Many theoretical and experimental studies suggested that the exact route is related to the special catalyst used. The O–H scission was proposed theoretically as the initial dissociation step over metal oxide (MgO, TiO_3, SnO_2, and CeO_2) [12–14] and metal carbide (Mo_2C) [15] catalysts, while C–H scission was more favorable than O–H scission on Pt (1 1 1) catalyst [16,17]. Among the three routes, the C–O scission is suggested to be the impossible one by both experimental [18] and theoretical [19,20] studies.

MoS_2 exhibits similar properties as noble metals and excellent catalytic behavior in several reactions, especially for hydrodesulfurization (HDS) and hydrogenation (HYD). A large number of experimental [21–25] and theoretical [26–34] studies were carried out to find the active sites on the catalyst surface and to examine the reaction mechanisms involved in HDS and HYD. Recently, CO hydrogenation was studied by using density functional theory (DFT); Huang and Cho [35] revealed that CH_xO was the intermediate to produce CH_4 on stoichiometric MoS_2 surface, while Shi et al. [36] found that CH_2OH is the intermediate prior to produce CH_4 on the non-stoichiometric MoS_2 surfaces.

Although the experimental studies suggested that methanol as the primary product from CO hydrogenation [10,11] could undergo secondary reactions to produce methane or higher alcohols, the mechanism of methanol decomposition on MoS_2 is still not fully understood. In this work, the adsorption and subsequent dissociative reaction of methanol on MoS_x clusters were investigated by using DFT. The pathways of C–H, C–O and O–H bond scission were considered. The construction and geometries of MoS_x models were described and the adsorption and dissociation of methanol over bald Mo-edge, 50% Mo-edge, and 50% S-edge were examined.

2. Models and methods

2.1. Models

MoS_2 catalyst has a closely packed layered sandwich structure with each Mo atom coordinated by six sulfur atoms in a prismatic unit, and Mo atoms are in a plane situated between two sulfur layers [37]. The high-resolution scanning tunneling microscopy revealed that the overall morphology of MoS_2 nanoparticle is sensitive to reaction conditions [38]. MoS_2 nanocluster with triangular morphology is predominant at an atmosphere of $H_2S/H_2 = 500$, whereas it is converted to the hexagonally truncated structure

* Corresponding author. Tel.: +86 351 4046092; fax: +86 351 4041153.
E-mail address: iccjgw@sxicc.ac.cn (J. Wang).

1381-1169/$ – see front matter © 2011 Elsevier B.V. All rights reserved.
doi:10.1016/j.molcata.2011.01.024

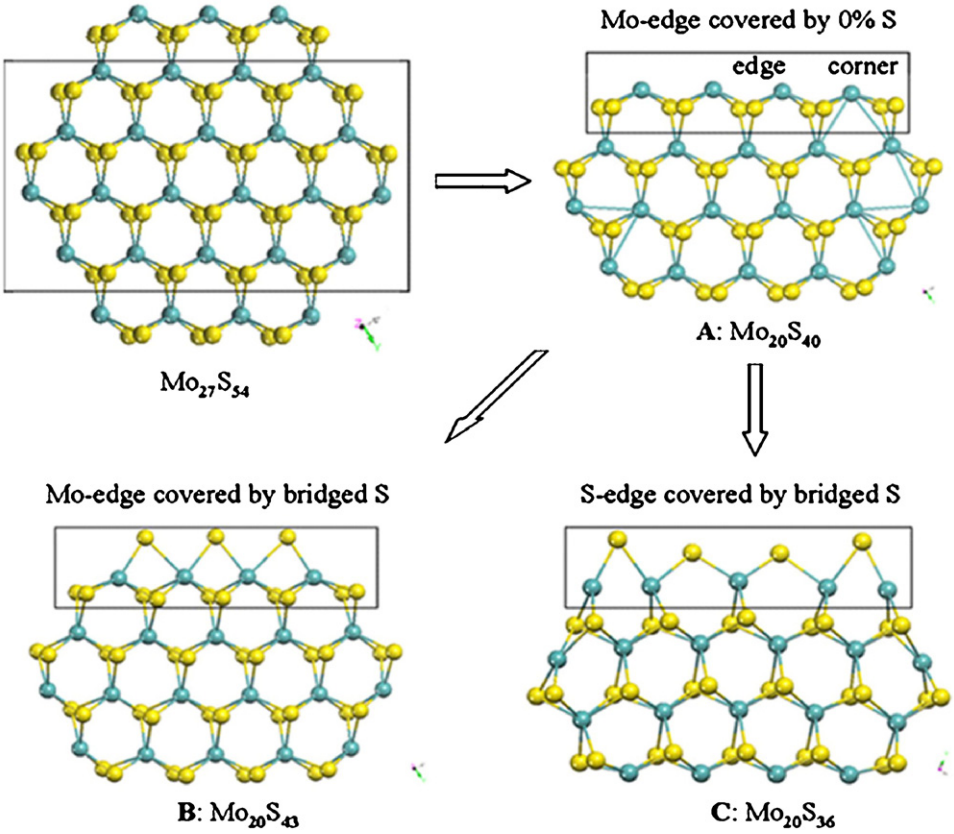

Fig. 1. Optimized structures of (A) $Mo_{20}S_{40}$, (B) $Mo_{20}S_{43}$ and (C) $Mo_{20}S_{36}$ deduced from $Mo_{27}S_{54}$ (blue: Mo; yellow: S). (For interpretation of the references to color in this figure legend, the reader is referred to the web version of the article.)

by sulfurating at an atmosphere of $H_2S/H_2 = 0.07$. As the existence of S is usually infrequent and hydrogen is abundant when it comes to the methanol conversion and dissociation processes, the hexagonal MoS_2 nanocluster is subjected in the present work. The lattice of hexagonal MoS_2 is of a layer type with weakly coupling MoS_2 sheets oriented along the (0 0 0 1) direction. Each MoS_2 sheet consists of two differently terminated layers, i.e. Mo and S termination, which may offer the active sites for the catalytic reactions.

It is experimentally demonstrated that the particles size of active MoS_2 is in the range of 10–30 Å in the highly dispersed supported catalysts [39]. Theoretic studies demonstrated that $Mo_{27}S_{54}$ cluster, with a diameter of 19 Å, is comparable to the size of real catalyst particle [40–42]. Our preliminary work proved that a simplified $Mo_{20}S_{40}$ cluster is effective enough in modeling the adsorption of methanol [43]. In addition, the sulfur coverage of MoS_2 surface is also sensitive to reaction conditions, especially the ratio of H_2S/H_2. It was reported that both the addition of sulfur to bare Mo edge and the removal of sulfur from full covered S-edge are exothermic; the MoS_x configuration with sulfur atoms bridging two neighboring Mo atoms (50% Mo-edge and 50% S-edge) is stable under high reductive conditions ($H_2S/H_2 < 0.01$) [27,28,44,45], while bare Mo edge (0% Mo-edge) may become stable under a lower reductive conditions ($0.01 < H_2S/H_2 < 0.07$). MoS_2 surfaces with different sulfur coverages may have a great effect on the methanol adsorption and dissociation. In this work, therefore, the stoichiometric cluster of $Mo_{20}S_{40}$ (0% Mo-edge) (**A**) as well as the nonstoichiometric clusters such as $Mo_{20}S_{43}$ (50% Mo-edge) (**B**) and $Mo_{20}S_{36}$ (50% S-edge) (**C**) are all considered to investigate the adsorption and dissociation of methanol on MoS_x clusters, as shown in Fig. 1.

2.2. Methods

All calculations were performed with the program package DMol^3 in the Materials Studio 2.2 of Accelrys Inc. [46–48]. The generalized gradient approximation (GGA) corrected functional by Perdew and Wang (PW91) [49] was employed, and the real space cutoff of atomic orbital was set at 5.5 Å. In DMol^3 the physical wave functions were expanded in terms of accurate numerical basis sets. For structure optimizations and energy calculations, the effective core potential (ECP) was used on molybdenum atoms, while the doubled numerical basis set with *p*- and *d*-polarization functions was used for all other elements. The tolerances of energy, gradient, displacement, and self-consistent field convergence are 2×10^{-5} au, 4×10^{-3} au/Å, 5×10^{-3} Å, and 1×10^{-5} au, respectively.

The medium quality mesh size was used for the numerical integration, and a Fermi smearing of 0.0005 au was used to count the orbital occupancy. The Linear Synchronous Transit/Quadratic Synchronous Transit method at the same level was used in searching for transition states (TS). The vibrational frequency of possible TS was calculated, and each TS was identified to have one imaginary frequency.

To describe the interaction between the adsorbates and the substrates, the adsorption energy was defined in Eq. (1), where *E*(cluster), *E*(adsorbates) and *E*(adsorbates/cluster) represent the energies of optimized cluster, gas-phase adsorbates and adsorbates–cluster complex, respectively. The spin-polarization calculation in gas species and adsorption systems with open shell character were considered:

$$E_{ads} = E\left(\text{adsorbates/cluster}\right) - E(\text{adsorbates}) - E(\text{cluster}) \quad (1)$$

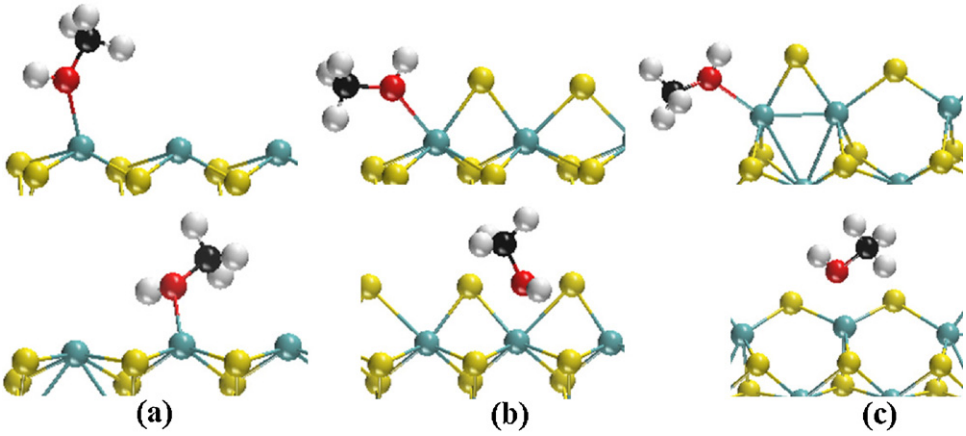

Fig. 2. Optimized methanol molecular structures on clusters A, B and C (blue, Mo; yellow, S; black, C; red, O; light, H). The upper row indicates methanol adsorbed on the corner sites and the lower one is methanol adsorbed on the edge sites. (For interpretation of the references to color in this figure legend, the reader is referred to the web version of the article.)

Table 1
Calculated adsorption energies and geometric parameters for one methanol molecule adsorbed on the clusters A, B and C of MoS_x.

Entry	Mode	E_{ads} (eV)	R_{Mo-O} (Å)	R_{C-O} (Å)
1	Corner/A	−1.27	2.18	1.46
2	Edge/A	−1.17	2.22	1.46
3	Corner/B	−0.94	2.22	1.46
4	Edge/B	−0.13	3.62	1.43
5	Corner/C	−1.00	2.27	1.45
6	Edge/C	−0.58	2.37	1.45

A non-symmetric slab system charge rearrangements may result in large dipole that affected the accuracy of the adsorption energies E_{ads} [36]. For the cluster system, however, the adsorbed molecule breaks the dipole existence; the effect of dipole correction is then presumed very small and can be ignored. This was verified in the test calculations for the adsorption of acetyl and CH_3CO on Mo-edge and S-edge by employing the Vienna ab initio simulation package (VASP) [50,51] in the preliminary work [43].

3. Results and discussion

3.1. Adsorption of methanol

The dissociation of methanol begins with its adsorption from the gas phase. A methanol molecule is top adsorbed on the corner and edge sites, as shown in Fig. 2. Table 1 lists the calculated structure parameters and adsorption energies of methanol molecule adsorbed on the clusters **A**, **B**, and **C** of MoS_x.

Model A ($Mo_{20}S_{40}$): As given in Table 1, forms 1 and 2 denote the configurations of one methanol molecule adsorbed on corner Mo (Mo_c) and edge Mo (Mo_e) sites, respectively. The adsorption energies on Mo_c and Mo_e are −1.27 and −1.17 eV, respectively; it indicates that the adsorption of methanol on cluster **A** is strongly exothermic and Mo_c is slightly higher active for methanol adsorption than Mo_e. The distances of C–O bond in methanol molecule adsorbed on corner and edge sites are nearly the same, while the distance of Mo_c–O is a little shorter than that of Mo_e–O. It indicates that the interaction of methanol with Mo_c is slightly stronger than that with Mo_e. The calculated C–O distance of methanol in gas-phase is 1.43 Å, equal to the data obtained by Yudanov et al. [19]; this confirms that the method used in this work is reasonable. The C–O distance is elongated from 1.43 Å in free methanol molecule to 1.46 Å in the adsorption complex.

Model B ($Mo_{20}S_{43}$): Forms 3 and 4 in Table 1 denote the configurations of one methanol molecule adsorbed on the Mo_c and Mo_e sites of model B, with the E_{ads} values of −0.94 and −0.13 eV, respectively. The corner site shows much higher activity for methanol adsorption than the edge site. This large difference can be rationally explained by the structural diversity of Mo-edge. The Mo_c atom in B coordinated by five S atoms is unsaturated, while the Mo_e is saturated by coordination with six bridged-S atoms. It suggests that the Mo_c site is much easier to be bonded with the adsorbates. The higher activity of Mo_c site can also be supported by the distances of Mo–O and C–O bonds. The Mo_c–O and Mo_e–O distances are 2.22 and 3.62 Å and the corresponding C–O distances are 1.46 and 1.43 Å, respectively. The C_e–O distance is equal to that of gas-phase methanol (1.43 Å), about 0.03 Å shorter than the C_c–O distance. The higher activity of Mo_c site for methanol adsorption may be ascribed to its unsaturated coordination statues.

Model C ($Mo_{20}S_{36}$): The Mo_c atom centered in model C is coordinated by three S atoms and is thus 3-fold unsaturated, while the Mo_e is coordinated by four S atoms and is 2-fold unsaturated. Forms 5 and 6 denote the configurations of one methanol adsorbed on Mo_c and Mo_e of model C, with E_{ads} of −1.00 and −0.58 eV, respectively. Analogous to model B, the corner site shows much higher activity for methanol adsorption, as suggested by the E_{ads}. The distances of Mo_c–O and C–O bonds are 2.27 and 1.45 Å, respectively. The distances of Mo_e–O and C–O bonds are 2.37 and 1.45 Å, respectively. Mo_c–O is 0.10 Å shorter than Mo_e–O, which is in accord with the E_{ads} values.

The above results suggest that the adsorption of methanol is much less stable on the edge sites than that on the corner sites, with the exception of model A. The corner Mo center and edge Mo center in model A are close in structural and electronic properties, leading to the almost the same adsorption energies. Therefore, we only consider the corner-Mo sites for the dissociative adsorption of methanol and its decomposition species in the following sections.

3.2. Adsorption of intermediates

Adsorbed methanol molecules can decompose in several steps to form various CH_xO and CH_x intermediates. Therefore, the adsorption of intermediates including methoxide (CH_3O), hydroxymethyl (CH_2OH), formaldehyde (CH_2O), methyl (CH_3) and methylene (CH_2) are calculated in the present work. The optimized structures of these intermediates adsorbed on the three clusters are shown in Fig. 3. The adsorption energies of the intermediates and the C–O

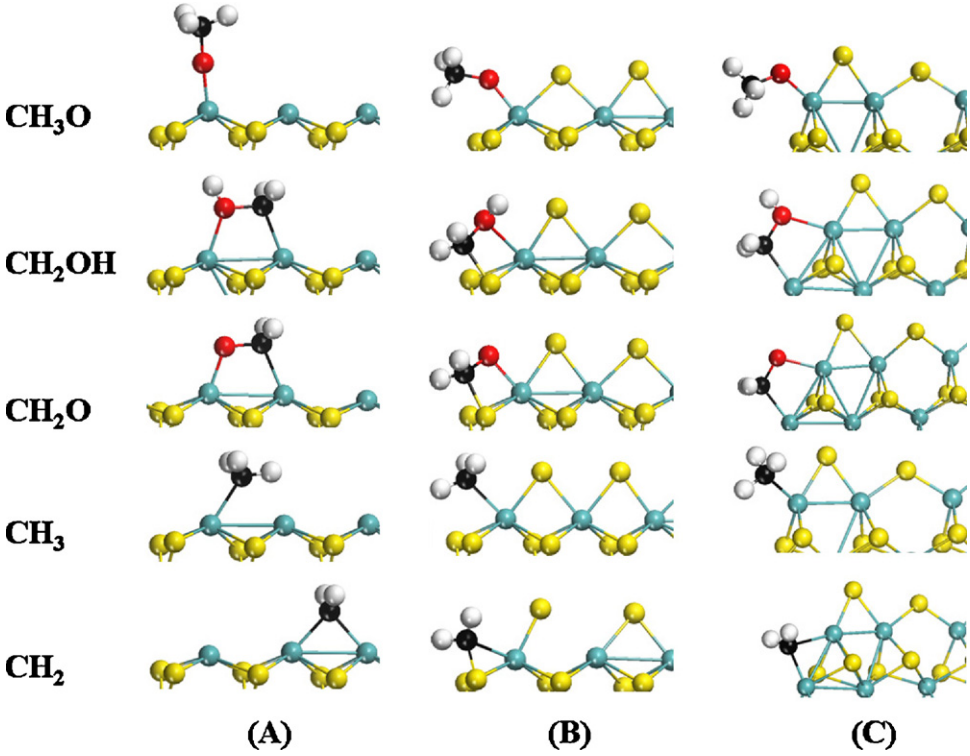

Fig. 3. Most stable configurations of some intermediates (CH_3O, CH_2OH, CH_2O, CH_3, and CH_2, from up to down) adsorbed on clusters A, B and C of MoS_x (blue, Mo; yellow, S; black, C; red, O; light, H). (For interpretation of the references to color in this figure legend, the reader is referred to the web version of the article.)

Table 2
Adsorption energies of several intermediates and the distances of C–O bond in the adsorbed and gas phase of these intermediates from methanol dissociation.

Intermediate	Adsorption mode	E_{ads} (eV)			Gas phase R_{C-O} (Å)	Adsorbed R_{C-O} (Å)		
		A	B	C		A	B	C
CH_3O	Top	−4.29	−2.77	−3.02	1.365	1.425	1.414	1.417
CH_2OH	η^2-(C,O)	−3.36	−2.38	−2.37	1.375	1.508	1.455	1.479
CH_2O	η^2-(C,O)	−2.90	−1.40	−1.81	1.212	1.462	1.378	1.445
CH_3	Top	−3.08	−1.83	−2.01	–	–	–	–
CH_2	Bridge	−5.09	−4.31	−4.15	–	–	–	–

distances in the adsorbed and gas phase of these intermediates are listed in Table 2.

Over model A, CH_3O is adsorbed on Mo_c in top mode through its oxygen atom, which accounts for an adsorption energy of −4.29 eV. The C–O bond in CH_3O is perpendicular to the Mo-edge. The C–O distance is 1.43 Å, elongated by 0.06 Å comparing with that in gas phase. The hydroxymethyl CH_2OH is formed via elimination of an H atom from the C center of methanol. CH_2OH is adsorbed in a η^2-(C,O) mode, in which C and O atoms bond to two Mo centers separately, with the adsorption energy of −3.36 eV. In CH_2OH, the C–O bond is parallel to the Mo-edge with the C–O distance of 1.51 Å, elongated by about 0.13 Å comparing with that in gas phase. It is noteworthy that the hybrid orbital of carbon is sp^3 in the adsorbed configuration, while sp^2 in the gas phase. Similar to CH_2OH, CH_2O is also adsorbed in η^2-(C,O) mode with the adsorption energy of −2.90 eV. The C–O distance is 1.46 Å, elongated by up to 0.25 Å comparing with that of 1.21 Å in the gas phase. It is presumed that the C–O bond is easy to break because of the large elongation of C–O bond length. CH_3 is adsorbed in a top mode which accounts for the adsorption energy of 3.08 eV. The dehydrogenation of CH_3 may continue to form CH_2, which is adsorbed in the bridged mode with the adsorption energy of −5.09 eV.

Over models B and C, all of these intermediates are strongly exothermic for the adsorption, indicating all of them are stable on MoS_2 surfaces. As shown in Fig. 3, CH_3O and CH_3 are adsorbed on corner Mo atom in a top mode; CH_2OH and CH_2O are adsorbed in a η^2-(C,O) mode on one Mo atom and one S atom over the cluster B, while on two Mo atoms over the cluster C. Moreover, CH_2 is bridge-adsorbed on one Mo atom and one S atom over the cluster B, while on two Mo atoms over the cluster C. It is found that the adsorption configurations of intermediates are almost the same as those on model A, but their adsorption energies are much smaller. The C–O distances in these adsorbed intermediates are slightly elongated comparing with that in the gas phase.

Through comparing these intermediates adsorbed over the three clusters, it is found that their adsorption stability is in the order of $CH_2 > CH_3O > CH_2OH > CH_3 > CH_2O$, which is consistent to the result of a slab model calculation of these intermediates on MoS_2 [36]. DFT calculations of various dehydrogenated intermediates (CH_3O, CH_2OH, CH_2O and CHO) on Pd (1 1 1) suggested that the most favorable configurations are CH_3O and CH_2OH species [19]. Moreover, the order of adsorption stability for CH_x species on Pd (1 1 1) is also consistent with the result in this work. It indicates that MoS_2 is similar to noble metal in the dissociative adsorption of methanol.

3.3. Methanol dissociation

To understand the properties and reactivity of methanol on MoS_2, the pathways of methanol dissociation via initial C–O, O–H

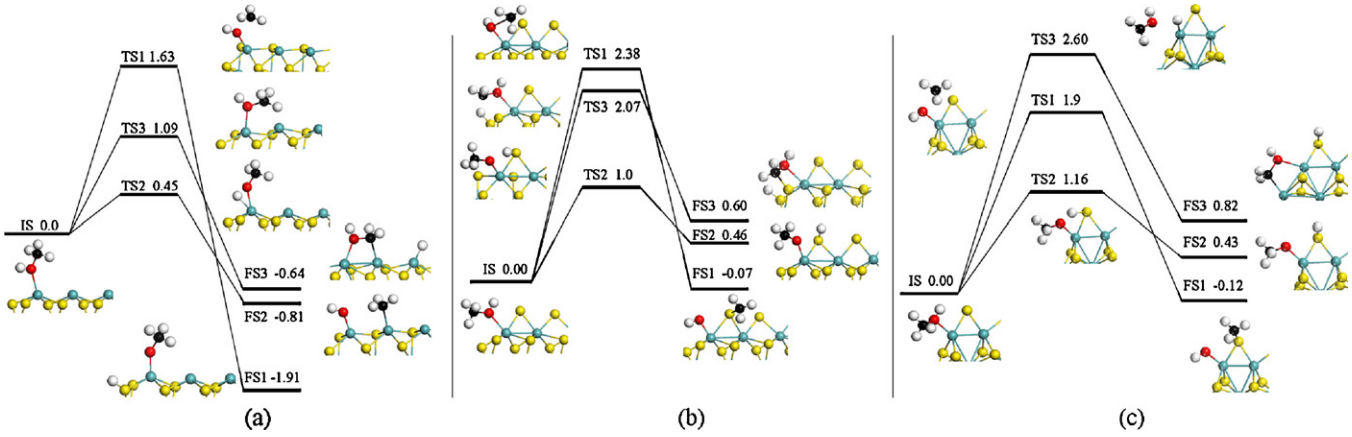

Fig. 4. Energy diagrams for methanol dissociation over clusters A, B and C (blue, Mo; yellow, S; black, C; red, O; light, H). For *TSx* and *FSx*, *x* = 1, 2, and 3 represent C–O, O–H, and C–H scission pathways, respectively. (For interpretation of the references to color in this figure legend, the reader is referred to the web version of the article.)

and C–H scissions and the pathways of intermediates dissociation on MoS_2 are systematically examined. The energy diagrams for methanol dissociation through C–O, O–H and C–H bond scission over the three clusters A, B and C are shown in Fig. 4. Here, *IS* represents the initial state (adsorbed methanol), *TSx* and *FSx* (*x* = 1, 2, 3) represent the transition states and the final states in the reactions of bond scissions (*x* = 1, C–O; 2, O–H; 3, C–H), respectively.

3.3.1. Methanol dissociation on model A ($Mo_{20}S_{40}$)

As shown in Fig. 4(a), the pathway of C–O scission is initiated via *TS1*, producing methyl (CH_3) and hydroxyl group (OH) (*FS1*). The carbon in methyl exhibits sp^2–like hybridization in *TS1*, while sp^3–like hybridization in *FS1*. The C–O length elongates considerably from 1.46 Å in *IS* to 2.22 Å in *TS1*. This reaction is highly exothermic by 1.91 eV with an energy barrier of 1.63 eV.

The pathway of O–H scission is initiated by the cleavage of the hydroxyl group via *TS2*, producing methoxide (CH_3O) (*FS2*). The hydrogen atom derived from the hydroxyl group is adsorbed on Mo_c in *TS2* and is transferred to S_c in *FS2*. The O–H length elongates considerably from 0.97 Å in *IS* to 1.30 Å in *TS2*. This reaction is exothermic by 0.81 eV with an energy barrier of 0.45 eV. The pathway of C–H scission starts with methanol dehydrogenation producing hydromethyl (CH_2OH). Methanol (*IS*) adsorbs on Mo-edge in a η^1-(O) mode (only O atom is bound to Mo), while methanol adsorption in *TS3* and *FS3* shows approximative η^2-(C,O) [19]. The C–H length elongates from 1.09 Å in *IS* to 1.40 Å in *TS3*. This reaction is exothermic by 0.64 eV with the lowest energy barrier of 1.09 eV.

Reaction energies and the activation barriers obtained here suggested that for the methanol dissociation on A, all three pathways (C–O, O–H and C–H scission) are highly exothermic and thermodynamically favorable. O–H scission to form the co-adsorbed methoxide and hydrogen is kinetically preferred on A. The activation barrier of the O–H scission is only 0.45 eV, much lower than the barriers of 1.09 eV for the C–H scission and 1.63 eV for C–O scission. Meanwhile, C–O scission is unfavorable although it produces the most stable product states.

3.3.2. Methanol dissociation on model B ($Mo_{20}S_{43}$)

As shown in Fig. 4(b), the energy barriers of C–O and C–H scission on cluster B are 2.38 and 2.07 eV, respectively. C–O scission is slightly exothermic or thermoneutral (−0.07 eV), while C–H scission is endothermic (0.60 eV). The hybrid orbital of C atom converts to sp^2-like in *TS1*. The C–O distance in *TS1* is 2.26 Å. The product CH_3 in *FS1* is adsorbed on the bridged S atom. The C–H distance in *TS3* is 1.79 Å. CH_2OH (*FS3*) is adsorbed in η^2-(C,O) mode binding to Mo_c (corner-Mo) and S_o (outer-S) [28]. O–H scission is the most favorable pathway which requires the lowest energy barrier of 1.0 eV. The O–H distance in *TS2* is 1.67 Å. The hydrogen derived from hydroxyl group is transferred to corner bridged-S.

3.3.3. Methanol dissociation on model C ($Mo_{20}S_{36}$)

As shown in Fig. 4(c), the energy barriers of C–O and C–H scission on cluster C are 1.90 and 2.60 eV, respectively. C–O scission is slightly exothermic or thermoneutral (−0.12 eV), while C–H scission is highly endothermic (0.82 eV). The distances of C–O in *TS1* and C–H in *TS3* are 2.35 and 1.81 Å, respectively. The hybrid orbital of carbon atom in *TS3* is sp^2-like. O–H scission requires the lowest energy barrier of 1.16 eV and the O–H distance in *TS2* is 1.67 Å. It indicates that O–H scission is the most favorable reaction route for methanol dissociation on cluster C, which is consistent with the results for the clusters A and B.

3.4. Dissociation of intermediate species

To identify the possible intermediates formed during methanol dissociation, the formation and dissociation of the resulting CH_3, CH_3O and CH_2OH species on the clusters A, B and C are shown in Fig. 5.

As shown in Fig. 5(a), the overall reaction of methanol decomposition is thermodynamically favorable on cluster A. Methoxide produced from methanol dissociation may continue to dissociate via C–O bond breaking to produce methyl with the energy barrier of 1.69 eV, while methoxide dissociation via C–H bonds is impossible with a high energy barrier up to 4.00 eV (not shown in Fig. 5). The C–O distance in the transition states for producing CH_2OH during C–H scission (Fig. 4) is 1.53 Å, which is 0.16 Å (16 pm) longer than that in the gas phase. This large elongation of C–O length supports that C–O breaking in CH_2OH is favorable to produce CH_2 and hydroxyl. Consistently, the calculated energy barrier of C–O breaking of CH_2OH is small (0.35 eV), which is close to the result (0.31 eV) by slab calculation [35]. However, the O–H breaking of CH_2OH to form aldehyde (CH_2O) is unfavorable with an energy barrier of 1.75 eV. As shown in Fig. 5(a), the energy barriers of CH_3 formation from methanol and methoxide are comparable, and then the formation of CH_2 via elimination of one H atom of CH_3 requires 0.66 eV. The breaking C–H distance is 1.64 Å.

Although the formation of CH_2 from CH_2OH needs the lowest energy barrier of 0.35 eV, the initial elementary step of O–H scission of methanol dissociation producing methoxide is much more favorable than C–H scission producing CH_2OH. The reaction rates can be estimated by the Arrhenius formula $r = \nu \exp(-E_a/k_BT)$. For the methanol dissociation over the cluster A, the activation barriers

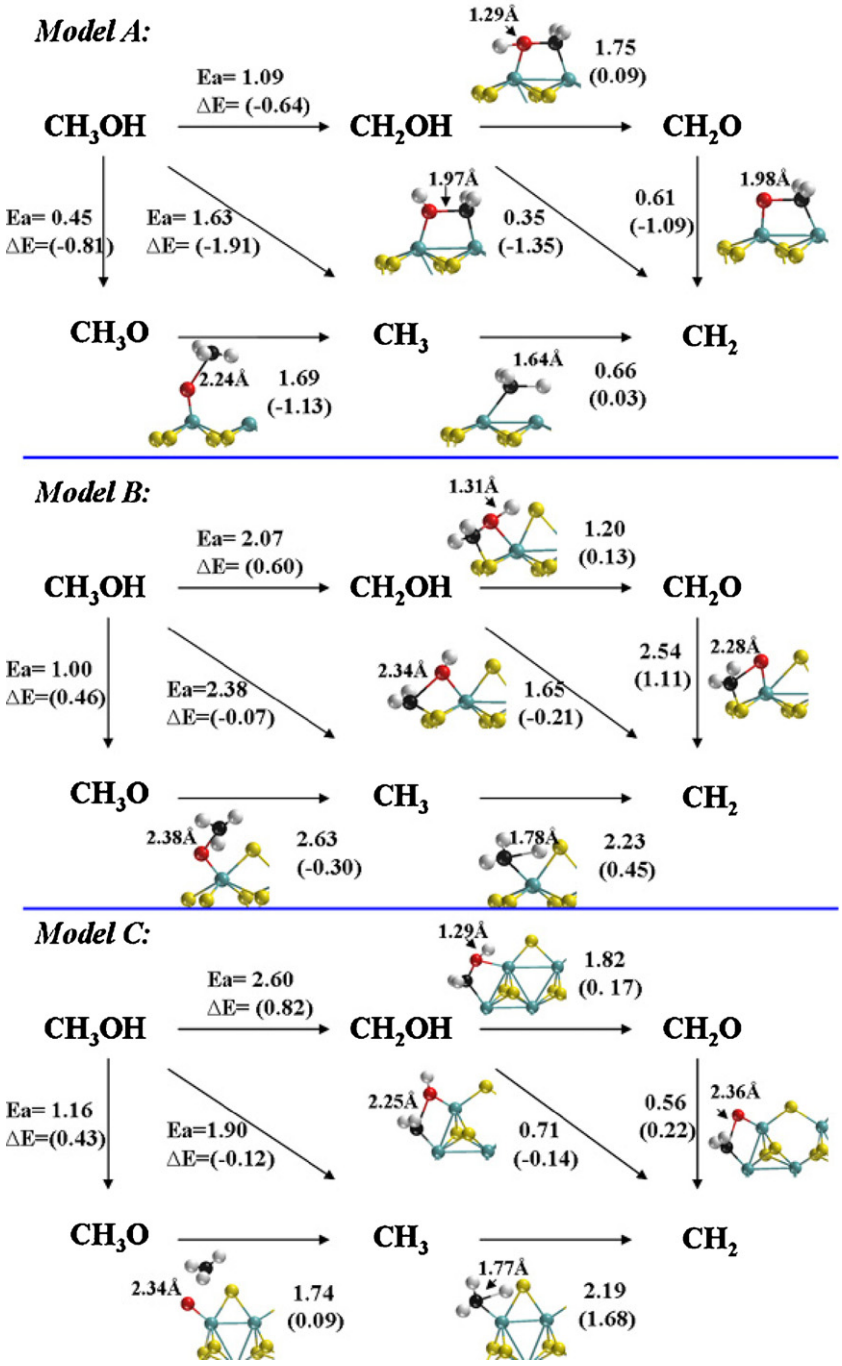

Fig. 5. Formation and dissociation of some intermediate species on clusters A, B, and C (blue, Mo; yellow, S; black, C; red, O; light, H). Reaction barriers (E_a) and heat of reactions (ΔE) are in the unit of eV. (For interpretation of the references to color in this figure legend, the reader is referred to the web version of the article.)

of the O–H scission and the C–H scission are 0.45 eV and 1.09 eV, respectively; by assuming a standard value of pre-exponential factor ($\nu \approx 10^{13}$), such a difference in the activation barrier will lead a reaction rate ratio of two pathways r(O–H)/r(C–H) = 3.3×10^4 at 714 K used for CO hydrogenation [52]. This indicates that the reaction rate of O–H scission is much faster than that of the C–H scission and the latter may then be negligible for the methanol dissociation. On the contrast, although the energy barrier of 1.69 eV for the reaction of CH_3O to CH_3 may look very high, it is still possible to be overcome under reasonable reaction conditions if there is no other better substitute; the reaction rate reaches 1.0 s^{-1} at 629 K with E_a = 1.69 eV, suggesting that it is considerable under the typical CO hydrogenation conditions. As a result, we may conclude that the favorable pathway of CH_2 formation is $CH_3O \rightarrow CH_3 \rightarrow CH_2$.

As shown in Fig. 5(b), the overall reaction of methanol decomposition is thermodynamically unfavorable on cluster B. CH_3 formation from CH_3O and its dissociation to CH_2 are unfavorable with high energy barriers of 2.63 and 2.23 eV, respectively. Different to that on the cluster A, CH_2OH on the cluster B prefers to form aldehyde via the O–H breaking rather than to form CH_2 via the C–O breaking, aldehyde is however not favorable for producing CH_2.

On the cluster C, as shown in Fig. 5(c), C–H scission is the most thermodynamically and kinetically unfavorable path. The energy barrier and reaction energy of O–H scission on the cluster C are similar to those on the cluster B. The breaking of C–O bond in CH_3O

on the cluster C requires an energy barrier of 1.74 eV, which is close to that on cluster A; however, the reaction of CH_3 to CH_2 on the cluster C is thermodynamically and kinetically unfavorable, indicating that the possible intermediate on cluster C is CH_3 rather than CH_2.

As comparing the methanol dissociations over the three clusters of MoS_2, it is found that the cluster A is the most active one with the lowest energies, while the relative orders of thermodynamic feasibility for the three possible bond scission routes are the same: C–O > O–H > C–H. However, three clusters are different in the feasibility order based on the bond breaking barrier; over the Mo-edge (A and B clusters), the feasibility is in the order of O–H > C–H > C–O [20], while over the S-edge (C cluster) it is in the order of O–H > C–O > C–H. It is obvious that O–H scission is the most favorable pathway on the MoS_2 surface. The C–O scission, for which the smallest activation barrier is 1.63 eV, is unfavorable on the MoS_2 surface. Thus, the reaction of C–O scission is probably restricted, consistent with the results obtained on Rd (1 1 1) [19].

It is interesting to note that C–H scission on C cluster is the least favorable pathway, possibly due to the steric hindrance. The transition state for the C–H bond breaking is highly strained and then the hybrid orbital of carbon atom in the transition state has to be sp^2-like. When the H atom adsorbed on corner Mo in the transition state is transferred to corner S in the final state, the product CH_2OH is bridged on two Mo atoms in which the hybrid orbital of carbon atom in the final state turns to be sp^3.

For the intermediates from methanol dissociation, it can be concluded that the possible intermediates are CH_3O, CH_3 and CH_2 on the cluster A while they are CH_3O and CH_3 on the cluster C. Because O–H scission is kinetically most favorable among the three bond-scissions and the energy barrier for the C–H scission producing CH_2OH is relatively higher, methoxide is the dominant surface species after the MoS_2 surface is exposed to methanol; this is consistent with the result of methanol adsorption on the CeO_2 (1 1 1) surface [14].

4. Conclusions

DFT calculations were carried out to investigate the methanol adsorption and dissociation through three pathways of C–O, O–H and C–H scission on $Mo_{20}S_{40}$ (0% Mo-edge), $Mo_{20}S_{43}$ (50% Mo-edge), and $Mo_{20}S_{36}$ (50% S-edge). The reactivity of several intermediate species from methanol dissociation was also identified. The results showed that methanol molecule adsorbed is much more stable on the corner sites than on the edge sites of $Mo_{20}S_{43}$ and $Mo_{20}S_{36}$. The adsorption stability order of the intermediate species adsorbed on MoS_2 surface is $CH_2 > CH_3O > CH_2OH > CH_3 > CH_2O$.

For methanol dissociation, the favorable bond scission order is O–H > C–H > C–O on the Mo-edge over $Mo_{20}S_{40}$ and $Mo_{20}S_{43}$, while it is O–H > C–O > C–H on the S-edge ($Mo_{20}S_{36}$). O–H bond scission is found to be the most favorable pathway on MoS_2 surface; the activation barrier is 0.45 eV on the bald Mo-edge and about 1.0 eV on the 50% Mo-edge and 50% S-edge. Among the intermediates formed from methanol dissociation, CH_2 is the most thermodynamically stable intermediate and CH_2 formation through $CH_3O \rightarrow CH_3 \rightarrow CH_2$ is favorable. For the dissociation of intermediates, CH_3O is the dominant surface species after the MoS_2 surface is exposed to methanol.

Acknowledgments

The authors are grateful for the financial support of the National Basic Research Program of China (2011CB201406, 2010CB226906) and the National Natural Science Foundation of China (10979068, 20876163) and the Knowledge Innovation Program of the Chinese Academy of Sciences (KJCX2.YW.H16, YZ200933).

References

[1] B.A. Peppley, J.C. Amphlett, L.M. Kearns, R.F. Mann, Appl. Catal. A 179 (1999) 31.
[2] A. Hamnett, Catal. Today 38 (1997) 445.
[3] H. Li, J. Li, F. Xiao, W. Wei, Y. Sun, J. Fuel Chem. Technol. 37 (2009) 613.
[4] Y. Usami, K. Kagawa, M. Kawazoe, Y. Matsumura, H. Sakurai, M. Haruta, Appl. Catal. A 171 (1998) 123.
[5] D.J. Elliot, F. Pennella, J. Catal. 114 (1988) 90.
[6] E.M. Calverley, K.J. Smith, Stud. Surf. Sci. Catal. 73 (1992) 111.
[7] M. Xu, E. Lglesia, J. Catal. 188 (1999) 125.
[8] M. Xu, E. Lglesia, Catal. Lett. 51 (1998) 47.
[9] J.G. Nunan, C.E. Bogdan, K. Klier, J. Smith, C.W. Young, R.G. Herman, J. Catal. 113 (1988) 410.
[10] M. Claeys, E. van Steen, Stud. Surf. Sci. Catal. 152 (2004) 601.
[11] K.G. Anderson, J.G. Ekerdt, J. Catal. 95 (1985) 602.
[12] M.A. Barteau, Chem. Rev. 96 (1996) 1413.
[13] M. Calatayud, A. Markovits, M. Menetrey, B. Mguig, C. Minot, Catal. Today 85 (2003) 125.
[14] D. Mei, N.A. Deskins, M. Dupuis, Q. Ge, J. Phys. Chem. C 112 (2008) 4257.
[15] C. Pistonesi, A. Juan, A.P. Farkas, F. Solymosi, Surf. Sci. 602 (2008) 2206.
[16] S.K. Desai, M. Neurock, K. Kourtakis, J. Phys. Chem. B 106 (2002) 2559.
[17] J. Greeley, M. Mavrikakis, J. Am. Chem. Soc. 126 (2004) 3910.
[18] O. Rodríguez de La Fuente, M. Borasio, P. Galletto, G. Rupprechter, H.-J. Freund, Surf. Sci. 566 (2004) 740.
[19] I.V. Yudanov, A.V. Matveev, K.M. Neyman, N. Rösch, J. Am. Chem. Soc. 130 (2008) 9342.
[20] R. Schennach, A. Eichler, K.D. Rendulic, J. Phys. Chem. B 107 (2003) 2552.
[21] G.A. Vedage, R.G. Herman, K. Klier, J. Catal. 95 (1985) 423.
[22] J. Saussey, J.C. Lavalley, T. Rais, J. Chem. Soc. Chem. Commun. 5 (1982) 278.
[23] T.J. Mazanec, J. Catal. 98 (1986) 115.
[24] Y.L. Fu, K. Fujimoto, P.Y. Lin, K. Omata, Y.S. Yu, Appl. Catal. A 126 (1995) 273.
[25] B.C. Wiegand, C.M. Friend, Chem. Rev. 92 (1992) 491.
[26] A. Travert, C. Dujardin, F. Maugé, S. Cristol, J.F. Paul, E. Payen, D. Bougeard, Catal. Today 70 (2001) 255.
[27] M. Sun, A.E. Nelson, J. Adjaye, Catal. Today 105 (2005) 36.
[28] L.S. Byskov, J.K. Nørskov, B.S. Clausen, H. Topsøe, J. Catal. 187 (1999) 109.
[29] M.V. Bollinger, K.W. Jacobsen, J.K. Nørskov, Phys. Rev. B 67 (2003) 085410.
[30] P. Raybaud, J. Hafner, G. Kresse, S. Kasztelan, H. Toulhoat, J. Catal. 189 (2000) 129.
[31] S. Cristol, J.F. Paul, E. Payen, J. Phys. Chem. B 106 (2002) 5659.
[32] T. Zeng, X.D. Wen, G.S. Wu, Y.W. Li, H. Jiao, J. Phys. Chem. B 109 (2005) 2846.
[33] H. Orita, K. Uchida, N. Itoh, J. Mol. Catal. A 193 (2003) 197.
[34] P.G. Moses, B. Hinnemann, H. Topsøe, J.K. Nørskov, J. Catal. 248 (2007) 188.
[35] M. Huang, K. Cho, J. Phys. Chem. C 113 (2009) 5238.
[36] X.-R. Shi, H. Jiao, K. Hermann, J. Wang, J. Mol. Catal. A 312 (2009) 7.
[37] R.W.G. Wyckoff, Crystal Structure, vol. 1, 2nd ed., John Wiley & Sons, 1964, 280.
[38] J.V. Lauritsen, M.V. Bollinger, E. Lægsgaard, K.W. Jacobsen, J.K. Nørskov, B.S. Clausen, H. Topsøe, F. Besenbacher, J. Catal. 221 (2004) 510.
[39] C. Calais, N. Matsubayashi, C. Geantet, Y. Yoshimura, H. Shimada, A. Nishijima, M. Lacroix, M. Breysse, J. Catal. 174 (1998) 130.
[40] Y.-W. Li, X.-Y. Pang, B. Delmon, J. Phys. Chem. A 104 (2000) 11375.
[41] X. Ma, H.H. Schobert, J. Mol. Catal. A 160 (2000) 409.
[42] H. Orita, K. Uchida, N. Itoh, J. Mol. Catal. A 195 (2003) 173.
[43] Y.-Y. Chen, X. Zhao, X.-D. Wen, X.-R. Shi, M. Dong, J. Wang, H. Jiao, J. Mol. Catal. A 329 (2010) 77.
[44] X.D. Wen, T. Zeng, B.T. Teng, F.Q. Zhang, Y.W. Li, J.G. Wang, H. Jiao, J. Mol. Catal. A 249 (2006) 191.
[45] M. Sun, J. Adjaye, A.E. Nelson, Appl. Catal. A 263 (2004) 131.
[46] B. Delley, J. Chem. Phys. 92 (1990) 508.
[47] B. Delley, J. Phys. Chem. 100 (1996) 6107.
[48] B. Delley, J. Chem. Phys. 113 (2000) 7756.
[49] J.P. Perdew, Y. Wang, Phys. Rev. B 45 (1992) 13244.
[50] G. Kresse, J. Furthmuller, Comput. Mater. Sci. 6 (1996) 15.
[51] G. Kresse, J. Furthmuller, Phys. Rev. B 54 (1996) 11169.
[52] K. Fang, D. Li, M. Lin, M. Xiang, W. Wei, Y. Sun, Catal. Today 147 (2009) 133.